JOURNAL OF MATERIALS SCIENCE 26 (1991) 814–820

An HREM study of domain structures and grain boundaries in $Ca_4Al_6SO_{16}$

Y. G. WANG, H. Q. YE, K. H. KUO, X. J. FENG*, G. L. LAO*, S. Z. LONG*
Laboratory of Atomic Imaging of Solids, Institute of Metal Research, Academia Sinica, 110015 Shenyang, Peoples Republic of China

Several different kinds of domain structures formed during phase transformation have been observed by means of high-resolution electron microscopy (HREM) in $Ca_4Al_6SO_{16}$. They are $\langle 1\,1\,0\rangle$ 90° and 120° orientation variants and $\langle 1\,1\,0\rangle$ translation variants found in the superstructure. These orientation variants are related to the lost symmetries of matrix and the number of them can be predicted according to the Van Tendeloo's conclusion. In addition to these domain structures, the $\langle 1\,1\,0\rangle$ 180° rotation domain with the characteristic feature of non-stoichiometry and $\{1\,1\,0\}$ general domain have also been revealed in the matrix. The $\{1\,1\,0\}$ and $\{2\,1\,1\}$ small angle grain boundaries were studied as well.

1. Introduction

It is known that the single crystal is often present as grains separated by different kinds of planar interfaces, which is usually the consequence of a phase transformation, as a result the domain structures could be introduced widely in many metals and nonmetal synthetic materials or natural minerals [1–3]. For a long time, therefore, it has been the subject of much research, especially since electron-microscopic methods have become available to observe directly the different structural variants and extended studies have already been carried out on this phenomenon. The treatment of domain structures in terms of group theory has already been proposed by Van Tendeloo and Amelinkx [4]. By this method the number of orientation variants as well as the number of translation variants can be determined from the point groups and lattices of precipitate and matrix.

Structural images recorded with a high-resolution electron microscope can provide information of local structure at atomic resolution and therefore can be used to reveal different kinds of structural variation in crystals. During the last few years, the high resolution electron microscopy technique has been applied with great success to the studies of the crystallographic shear structures [5], block structures [6] and tunnel structures [7] of minerals and cement. The present paper reports high resolution electron microscopic observations of various kinds of domain structures and grain boundaries in $Ca_4Al_6SO_{16}$ (usually abbreviated as C_4A_3S).

The sample, having nominal composition of $3CaO:3Al_2O_3:CaSO_4$, was sintered at 1380 °C in platinum container for 8 h and cooled in air. X-ray analysis confirmed the presence of C_4A_3S. The crystals were ground in an agate mortar and dispersed in absolute alcohol. Thin fragments of the crystals were collected on a holey carbon film supported on a copper grid. High resolution observations were carried out at 200 kV using a JEM-200CX electron microscope equipped with a high-resolution top-entry goniometer stage. High-resolution structural images were recorded at a magnification of 3.8 to 8.5×10^5 times, using an objective aperture corresponding to a radius of 3.5 nm^{-1} in the diffraction pattern.

The simulated image calculations were performed using the multislice method with a program written by Ishizuka [8]. The following parameters were used. Spherical aberration coefficient 1.2 mm, slice thickness 0.455 nm, (along $\langle 0\,0\,1\rangle$ axis) and 0.54 nm (along $\langle 1\,1\,1\rangle$ direction), the focus spread due to chromatic aberration 7 nm, incident beam convergence 0.3 mrad, and the number of diffraction beams included in the dynamical diffraction calculation, 419 and 326. The images were computed for a range of thicknesses up to 20 slices over a defocus range of − 48 to − 80 nm. The series of computed images for varied defocus and specimen thickness agree quite well with the through focus experimental images along the different orientations. The results of image simulation also show that the image dots on the plane where inverse occupation of calcium atoms happened in Figs 7 and 8 will become brighter than those on the unchanged plane, therefore the superstructures could be read directly for the high resolution images [9].

2. Results and discussion

The crystal structure of C_4A_3S has been determined by single-crystal X-ray analysis [10]. This cement is body-centred cubic (space group $I\bar{4}3\,m$) and its unit cell dimension is $a = 0.919$ nm. The feature of atomic arrangement is that calcium occupies the two sets of 8c position with different occupations. Besides this basic

* *Also at* Wuhan University of Technology, Luoshi Road 14, Wuhan, Peoples Republic of China

0022–2461/91 $03.00 + .12

structure a superstructure introduced by periodic inverse occupations of calcium on the two sets of positions along a {1 1 0} plane has been found with orthorhombic lattice (space group Bmm2) and its unit cell parameters are $a' = 1.298$, $b' = 1.298$, $c' = 0.919$ nm [9]. The presence of this one-dimensional (1D) superstructure causes the phase transformation and destroys some symmetries of matrix. For example, the three-fold symmetry along the ⟨1 1 1⟩ directions cannot hold, therefore, the orientation variants related by the lost symmetries could be introduced according to the conclusion of Van Tendeloo *et al.* [4] and the total number of these orientation variants can be calculated from the order of point group of matrix divided by that of point group of the 1D superstructure. The orders of point group of matrix and 1D superstructure are 24 and 4, respectively, and thus the number of orientation variants possibly caused is equal to 24/4 = 6. These long periodic directions are actually corresponding to the all independent directions of ⟨1 1 0⟩ and the angles between them are 120° or 90°, respectively. The 120° orientation variants related by three-fold symmetry and 90° oriented variants by $\bar{4}$ symmetrical operation so that these variants could be observed easily along the ⟨1 1 1⟩ and ⟨0 0 1⟩ directions along which the symmetries were lost. We will introduce the 120° and 90° orientation variants in turn.

2.1. 120° orientation variants

The orientation variants related by lost three-fold symmetry could be possibly caused during the phase transformation from the cubic to orthorhombic system, and a possible configuration of one kind of such domain structure is shown in Fig. 1, where the two domain variants are related by 120° rotation operation around the [1 1 1] axis or the mirror reflection across the (1 10) plane. This domain structure, therefore, can also be treated as the (1 1 0) reflection twin. The observed image is shown in Fig. 2, in which the 120° orientation relationship between the two variants is confirmed by the inserted electron diffraction pattern (EDP) unambiguously and the interface between the oriented variants exhibiting zig-zag form is

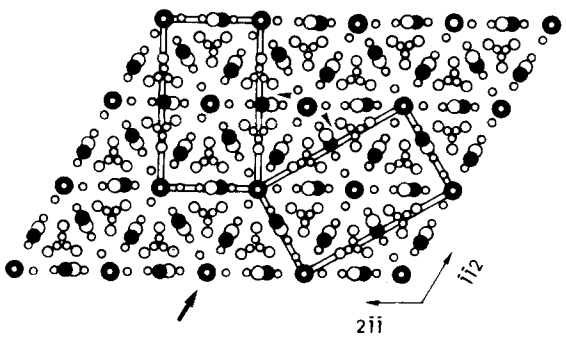

Figure 1 A possible structure model of ⟨1 1 0⟩ 120° orientation variants between the one-dimensional superstructure, where the largest to smallest circles represent sulphur, calcium, aluminium and oxygen atoms, respectively. The secondary large black circles are almost occupied by calcium, whereas the open ones almost vacancies.

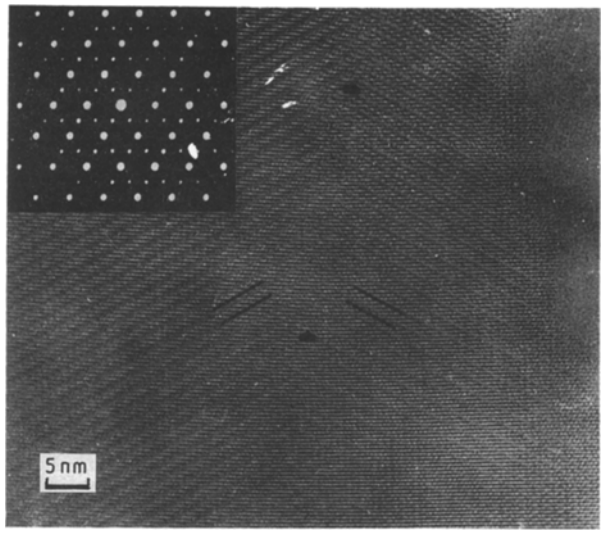

Figure 2 The [1 1 1] high resolution lattice image showing the ⟨1 1 0⟩ 120° orientation domains. The 120° orientation relationship between the two variants is confirmed by the inserted EDP and the interface indicated by arrows is in zig-zag form.

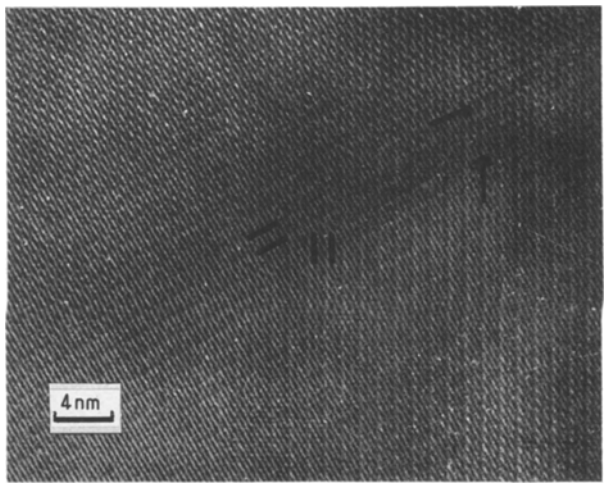

Figure 3 The [1 1 1] high resolution lattice image showing other arrangement of ⟨1 1 0⟩ 120° orientation variants comparing with Fig. 2.

matched very well with the suggested structural model. It should be noted two 120° rotation variants are not always related to the (1 1 0) reflection twin. Fig. 3 shows a little different arrangement of such 120° orientation domain structure, in which the two variants only related by rotating 120° around the [1 1 1] axis although it may give the same EDP as Fig. 2. The structure model of this domain structure is shown in Fig. 4. Fig. 5a shows the EDP which is similar with one of the three-dimensional superstructure, but the corresponding high resolution lattice image (Fig. 5b) exhibits three oriented variants related by the three-fold symmetry, these variants arrange irregularly and intersect with each other which may cause the streaking feature in the EDP (Fig. 5a). The intercrossing between them might possibly produce the two- or three-dimensional superstructures as well and these superstructures have been reported earlier elsewhere [9].

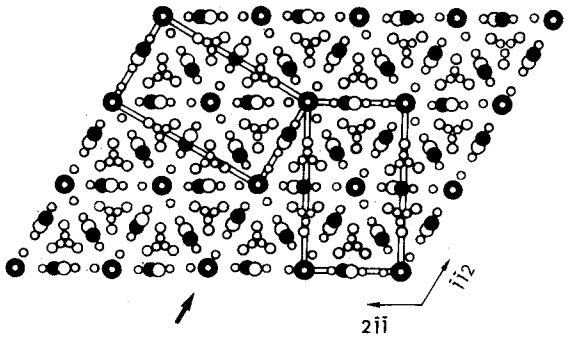

Figure 4 The [1 1 1] projected structure model of the ⟨1 1 0⟩ 120° orientation variants (see Fig. 3).

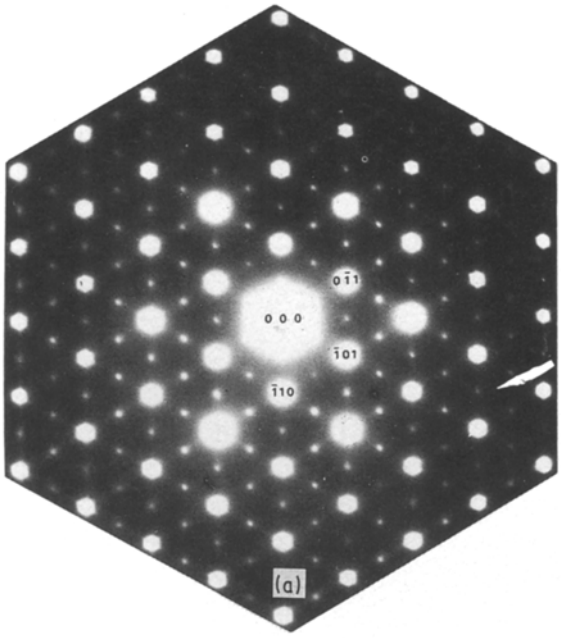

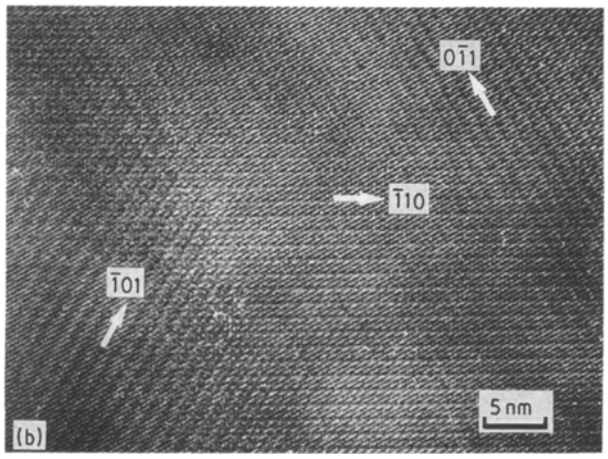

Figure 5 (a) An EDP with the beam parallel to the [1 1 1] direction showing pseudo three-dimensional superstructure and the streaks along ⟨1 1 0⟩ directions can be seen. (b) The corresponding high resolution lattice image showing three oriented variants related by three-fold symmetry, viewing along the arrows it can be seen clearly that they arrange disorderly and intersecting with each other.

2.2. 90° orientation domains

When the superstructure formed in the matrix of C_4A_3S, the $\bar{4}$ operation along the [0 0 1] direction will also be destroyed and as a result the two-fold symmetry could be present instead of $\bar{4}$ operation. Fig. 6 shows the experimental image, in which the two variants indicated by black lines at right angles can be seen clearly and this orientation relationship is also confirmed by the inserted EDP. This supplies evidence to support the above theoretic prediction. On the other hand such domain structure would also be understood very easily because {1 1 0} planes are all equal to each other and it is reasonable to predict that the periodic inverse occupation of calcium atoms on these planes could happen with equal possibility so that the coexistence of them may introduce the 90° or 120° orientation domain structures. It may be seen that these two perpendicular variants intersect each other at the centre area in Fig. 6 and thus the two-dimensional (2D) superstructure could be caused and the structure model of this 2D superstructure is shown in Fig. 7, where there is little difference from the earlier reported 2D superstructure [9].

In this case the 90° orientation variants may also be treated as the oriented twinning and thus the 120° and 90° twinnings may possibly be introduced in C_4A_3S during this phase transformation. As a result the interfaces separating the orientation variants are also called twin interfaces.

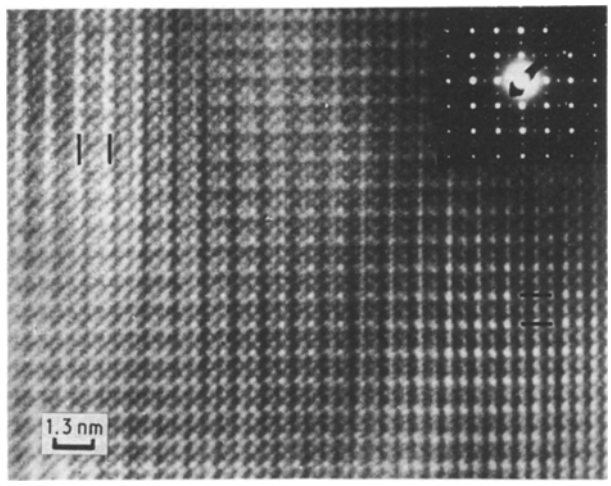

Figure 6 [0 0 1] structural image showing ⟨1 1 0⟩ 90° orientation variants indicated by lines, where two-dimensional superstructure formed by intercrossing of these two variants can be seen at the centre area.

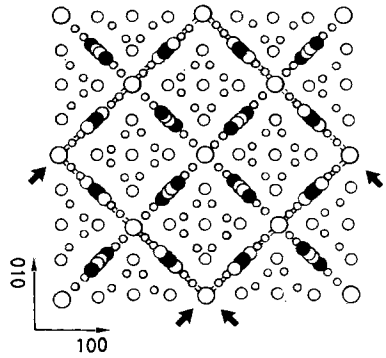

Figure 7 A [0 0 1] projection of the possible structure model of two-dimensional superstructure introduced by intercrossing of the ⟨1 1 0⟩ 90° orientation variants.

2.3. Translation variants

Besides the orientation variants, the translation variants may also be introduced during this phase transformation. In fact the number of different translation variants for a given orientation variant can also be calculated by the number of different translation vectors t which are lattice vectors for the matrix but not for the superstructure. All different t-vectors lead therefore from the origin of the unit cell of the superlattice to all lattice points within the primitive unit cell of the superlattice. This number can be obtained by dividing the volume of the primitive unit cell of the superstructure (v) by the volume of the primitive unit cell of the matrix (v_0). If non-primitive unit cells are used one should correct for the multiplicity; let m_1 and m_2 be, respectively, the multiplicities of the unit cells of the superstructure and superstructure, then $t = (m_1/m_2)(v/v_0)$ where $m_1 = m_2 = 2$ and we can obtain $t = 2$. The (1 1 1) projection of $\langle 1\,1\,0\rangle$ translation variants is shown in Fig. 8, in which the inverse occupation of calcium on $(0\,\bar{1}\,1)$ plane does not happen throughout the whole crystal but stopped mid way and the same thing happens in the next $(0\,\bar{1}\,1)$ plane, therefore there is a displacement of the superlattice along the [0 1 1] direction and the value of this displaceive vector R equals a half length of its cell axis. In other words, there is 180° phase difference between the two translation variants and one can call this the $[0\,\bar{1}\,1]$ antiphase domain in the superstructure. The experimental image is shown in Fig. 9, where such $[0\,\bar{1}\,1]$ translation variants can be seen clearly and they match well with the structure model shown in Fig. 8. The interface between the translation variants is the so-called translation interface.

2.4. $\langle 1\,1\,0\rangle$ 180° rotation domain in the matrix

If the part of crystal is rotated through 180° around the $\langle 1\,1\,0\rangle$ axis in the matrix, the rotation domain may be formed because the C_4A_3S matrix is a non-centrosymmetrical structure and the arrangement of atoms will be changed after such an operation. The possible structure models of domain structure built in such a way is suggested in Fig. 10. The domain boundaries are composed of double layers with the characteristic feature of non-stoichiometry so that these two layers are non-conservative and correspond to the excess or deficit of cations, respectively. Two kinds of connections of the inversion domains are shown in Figs 10a and 10b. In order to distinguish these two kinds of domain boundaries some areas at the interfaces are marked by asterisks in Fig. 10 and image simulation was also made in order to determine whether or not these areas would be imaged at certain imaging conditions. The simulated image was calculated based upon the structure model shown in Fig. 11a where the calcium and oxygen atoms located at the [1 1 1] and $[\bar{1}\,\bar{1}\,1]$ body diagonals in the unit cell are interchanged with each other and the results are exhibited in Figs 11b and 11c, respectively. From the image simulation it is known that the areas marked by asterisks at the interfaces could be imaged equally as those regular imaging positions under the Scherzer defocus and, therefore, such two kinds of non-conservative boundaries can be identified easily in the high resolution image by the different arrangements of the image dots at the interfaces. The experimental image demonstrating these domain structures is shown in Fig. 12, where at least five $(2\,\bar{1}\,\bar{1})$ domain boundaries arranged parallely can be recognized. By checking carefully the characteristic arrangement of image dots at these regains, the two kinds of interfaces can be distinguished from each other and indicated by the letters D and B, respectively. The dots pointed by the arrows at the interfaces correspond to the areas marked by asterisks in the structure model. In fact when these boundaries are introduced in a parallel arrangement, they must appear in an alternative way that can be found from the structure model. So that we only need to identify one of them and the next should be unambiguous. Viewing along the $[0\,\bar{1}\,1]$ direction as indicated in Fig. 12 the antiphase domain-like character may be found. Another feature of these interfaces is the ordering of them and thus the one-dimensional superstructure may be introduced along the $[2\,\bar{1}\,\bar{1}]$ direction and the repeat period of the superlattice is equal to the distance between the same kind of boundaries, where it is about 3.75 nm ($10d_{2\bar{1}1}$).

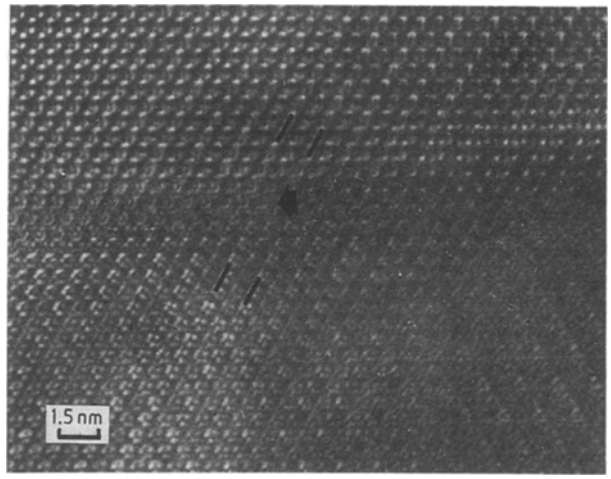

Figure 9 The [1 1 1] high resolution image showing the $[0\,\bar{1}\,1]$ translation variants which can be seen clearly from bottom to top, arrow indicates the translation interface.

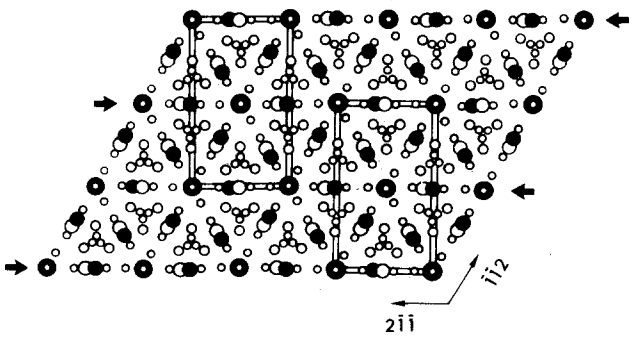

Figure 8 A possibly suggested [1 1 1] projection of the structure model of $\langle 1\,1\,0\rangle$ translation variants.

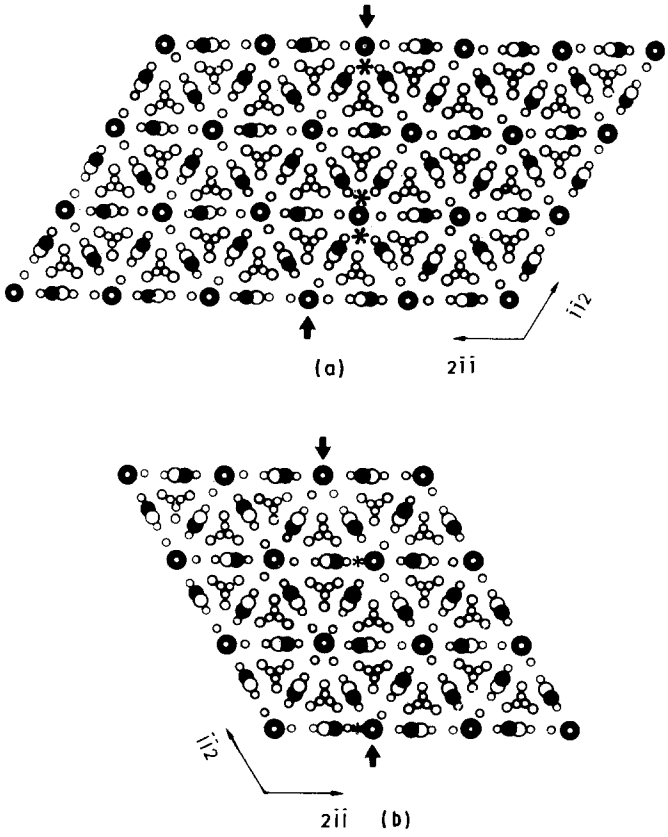

Figure 10 (a) and (b) are two kinds of possible ⟨1 1 0⟩ 180° rotation domain structure projected on the (1 1 1) plane, the domain interfaces are shown in arrows and the areas marked by asterisks can be used to identify the two kinds of interfaces in the structural image (Fig. 12).

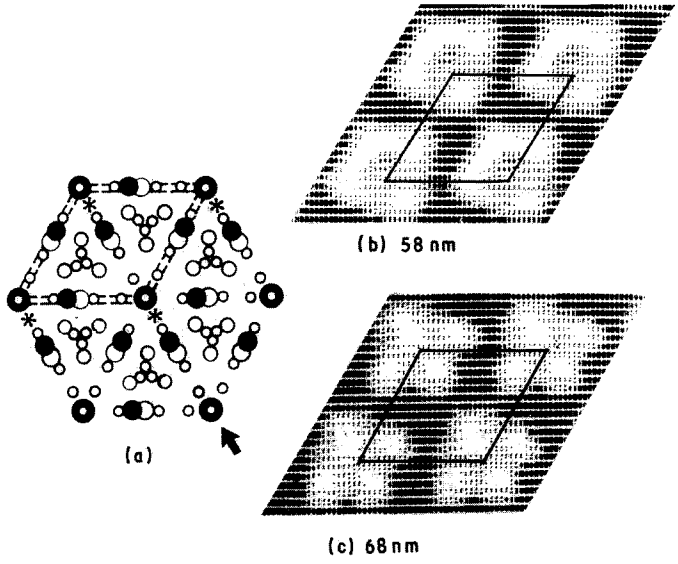

Figure 11 (a) A [1 1 1] projected structure model showing the interchange of atoms located on the [1 1 1] and [$\bar{1}\,\bar{1}$ 1] body diagonals and (b) and (c) are the simulated images calculated with 326 waves at a thickness of 5.4 nm and defocus values of 59 and 65 nm, respectively. The areas marked by asterisks in (a) could also be imaged at the Scherzer defocus.

2.5. {1 1 0} general domain

If the arrangement of atoms in this cement changes on a plane, for example (0 $\bar{1}$ 1) as shown in Fig. 13, the domain interface would be introduced. Here the configuration of the domain structure is obtained by twisting the top part of the crystal through 180° around the [0 $\bar{1}$ 1] axis and connecting it with the unchanged part. Although there is also 180° rotating around the [0 $\bar{1}$ 1] axis, the domain boundary in this case is different from that shown in Fig. 11 and we call it a (0 $\bar{1}$ 1) general domain interface. In other words, this domain interface also corresponds to the 180° twist grain boundary from the view of crystal dislocation. The observed high resolution image is shown in Fig. 14a, in which such a general domain boundary can be seen clearly at area D and matches very well with the structure model. The ordering of such domain boundaries is also found and exhibited in Fig. 14b, where they arrange parallely along the [0 $\bar{1}$ 1] direction so that the one-dimensional superstructure may be caused as well. The repeat period of this superstructure determined directly in the image is about 1.988 nm ($3d_{0\bar{1}1}$), therefore the superstructure introduced by the ordering of domain interface has been proved to be possibly present in the C_4A_3S.

2.6. Small angle grain boundaries in C_4A_3S matrix

The two crystals (namely, parts I and II) separated by small angle grain boundaries forming a bicrystal is

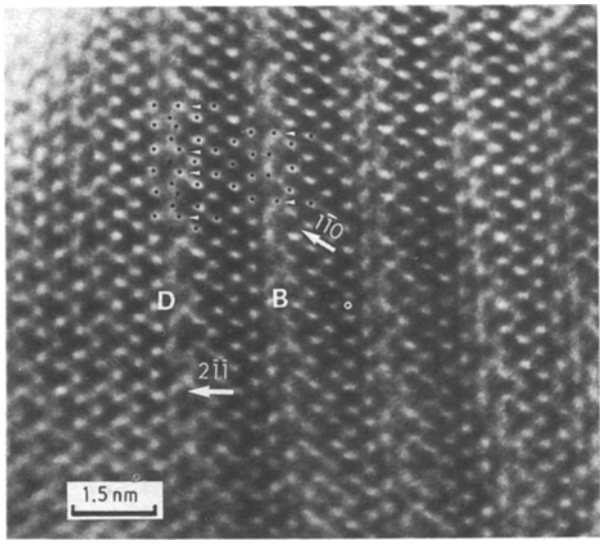

Figure 12 The [1 1 1] structural image showing the multiply ⟨1 1 0⟩ 180° rotation domain structure, the interfaces marked by D and B correspond to the structure models Fig. 11a and 11b, respectively.

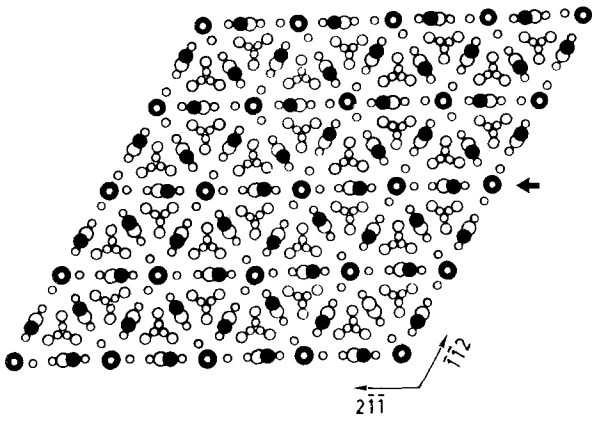

Figure 13 A possible structure model of {1 1 0} general domain projected upon the (1 1 1) plane, the arrow shows the domain boundary.

shown in Fig. 15, where the grain boundaries are parallel to the (0 $\bar{1}$ 1) and (2 $\bar{1}$ $\bar{1}$) planes known from the areas A and B, respectively. At area B the edge-dislocation wall can be seen clearly and faithfully coincident with the definition of small angle grain boundary. The misfit here is accommodated by atomic misfit on the boundary. The two grains have a common [1 1 1] axis and an angle difference in orientation is about 8° so that the Burgers vector b can be approximated by $\theta \times D$ and its value is very close to 1/6 [2 $\bar{1}$ $\bar{1}$]. The same analysis can also be used in area A.

The grain boundaries as well as those domain interfaces in cement clinker are sensitive areas to the hydration and, therefore the observed structural fluctuation may be favourable to improvement in its hydraulicity. As the defects contained in the clinker can increase the activity of hydration, which has been proved by treatment of neutron irradiation on the gamma phase of belite (Long *et al.* unpublished data), the defects in cement cannot be neglected.

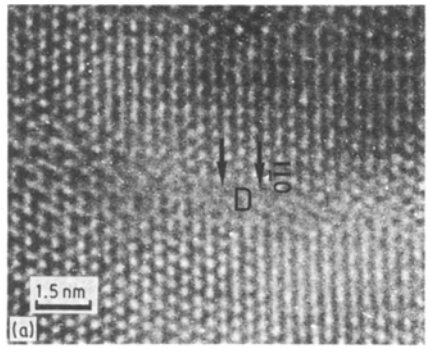

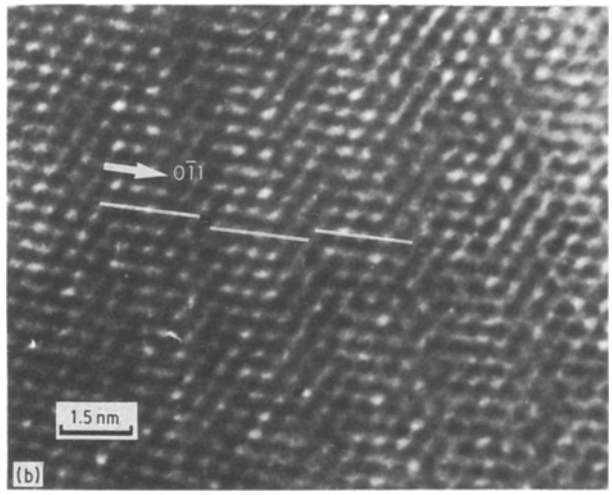

Figure 14 (a) The [1 1 1] structural image showing the (0 $\bar{1}$ 1) general domain structure at D and (b) the parallel arrangement of such domain boundaries along the [0 $\bar{1}$ 1] direction and as a result 1D superstructure may be introduced.

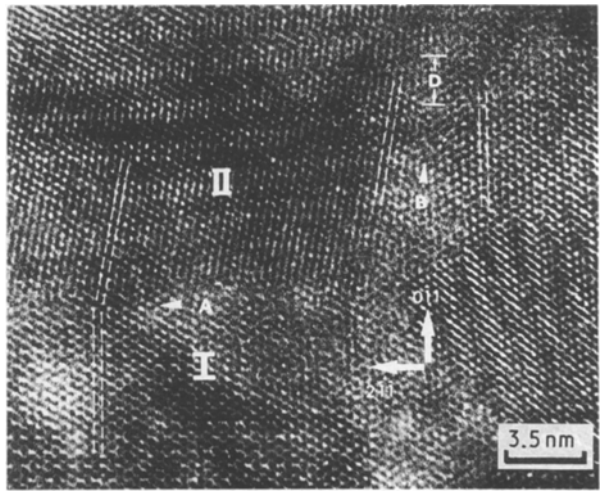

Figure 15 The [1 1 1] structural image showing the small angle grain boundaries, the grain boundary is parallel to the (0 $\bar{1}$ 1) plane at A and that parallel to (2 $\bar{1}$ $\bar{1}$) at B.

3. Conclusion

By using the technique of HREM the microstructures of C_4A_3S have been studied and many domain structures in the matrix as well as the one-dimensional superstructure have been observed. The corresponding structure models have also been suggested and the matches between the experimental results and proposed models are good. The feature of chemical

significance is the ordering of non-conservative boundaries. The relatively short-range (nanometres) fluctuations in ordering shown in Figs 12 and 14b indicate highly localized deviations from chemical equilibrium in this cement. The regular arrangements of non-conservative or conservative boundaries in this clinker show clearly the physical basis of its superstructure formation. On the other hand, the superstructures formed by the ordering of these interfaces are different from those revealed already. These results show that the microstructure of C_4A_3S could be very complicated and it is essential that the extent of these types of disorder is evaluated.

References

1. H. Q. YE, D. X. LI and K. H. KUO, *Phil. Mag.* **51** (1985) 839.
2. G. W. GROVES, *Cem. Concr. Res.* **12** (1982) 619.
3. P. R. BUSECK, "Review in Mineralogy", Vol. 7, "Pyroxenes", (Mineral Society of America, New York, 1981) p. 175.
4. G. VAN TENDELOO and S. AMELINKX, *Acta Crystallogr.* **A30** (1974) 431.
5. J. O. BOVIN, D. X. LI, L. STENBERG and H. ANNEHED, Proceedings 10th International Congress EM., Deutsche Gesellschaft für Elektronenmikyos-Kopie e.V. Hamburg, Vol. 3 (1982) 55.
6. S. TURNER and P. R. BUSECK, *Science* **212** (1981) 1024.
7. Y. G. WANG, B. S. ZOU, K. H. KUO and X. J. FENG et al., *J. Mater. Sci.* **24** (1989) 877.
8. K. ISHIZUKA, *Acta Crystallogr.* **A38** (1982) 773.
9. Y. G. WANG, H. Q. YE, K. H. KUO and X. J. FENG et al., *J. Mater. Sci.* **25** (1990) in press.
10. X. J. FENG, G. L. LAO and S. Z. LONG, *J. Chin. Solicate* (in Chinese) **18** in press.

Received 8 August 1989
and accepted 19 February 1990